INTERNATIONAL JOURNAL FOR NUMERICAL METHODS IN FLUIDS, VOL. 22, 1169–1187 (1996)

NUMERICAL STUDIES OF TRANSITIONAL TURBULENT PULSATILE FLOW IN PIPES WITH RING-TYPE CONSTRICTIONS

T. S. LEE, Z. D. SHI AND S. H. WINOTO

Mechanical and Production Engineering Department, National University of Singapore, 10 Kent Ridge Crescent, Singapore 0511

SUMMARY

Pulsatile flows in the vicinity of mechanical ring-type constrictions in pipes were studied for transitional turbulent flow with a Reynolds number (*Re*) of the order of 10^4. The Womersley number (*Nw*) is in the range 30–50, with a corresponding Strouhal number (*St*) range of 0·0143–0·0398. The pulsatile flows considered are a pure sinusoidal flow, a physiological flow and an experimental pulsatile flow profile for mechanical aortic valve flow simulations. Transitional laminar and turbulent flow characteristics in an alternating manner within the pulsatile flow fields were studied numerically. It was observed that fluid accelerations tend to suppress the development of flow disturbances. All the instantaneous maximum values of turbulent kinetic energy, turbulent viscosity and turbulent shear stress are smaller during the acceleration phase than during the deceleration period. Various parametric equations have been formulated through numerical experimentation to better describe the relationships between the instantaneous flow rate (Q), the pressure loss (ΔP), the maximum velocity (V_{max}), the maximum vorticity (ζ_{max}), the maximum wall vorticity ($\zeta_{w,max}$), the maximum shear stress (τ_{max}) and the maximum wall shear stress ($\tau_{w,max}$) for turbulent pulsatile flow in the vicinity of constrictions in the vascular tube. An elliptic relationship has been found to exist between the instantaneous flow rate and the instantaneous pressure gradient. Other linear and quadratic relations between various flow parameters were also obtained.

KEY WORDS: pulsatile flow; ring-type constrictions; turbulent flow

1. INTRODUCTION

The possibility that haemodynamic factors may participate in the genesis and proliferation of atherosclerosis has fostered increased study of flow through various types of constrictions during the past decade.[1] A recent research interest concerns the relationship between vascular disease and the effects of constrictions and the magnitude of wall shear stress. It is therefore worthwhile from the fluid dynamics point of view to study and identify regions of very high shear and normal stresses in the flow (haemolysis), regions of very low or very high shear stress at walls (atheromatous lesions) and the extent of separated or reversed flow regions (thrombosis) in vascular pipes.

For non-ring-type constrictions in vascular pipes, research investigations are numerous.[2–11] Studies on the characteristics of unsteady flow in the vicinity of ring-type constrictions in vascular pipes are of interest to designers of artificial heart valves and miniature pulsatile blood flowmeters.[12] The relation between unsteady flow rate and pressure loss across constricted ring-type devices can provide the means of estimating the resultant flow rate from the measured unsteady pressure losses. The characteristics of unsteady/pulsatile turbulent flows observed can also be used to improve the transportation of non-

CCC 0271–2091/96/121169–19
© 1996 by John Wiley & Sons, Ltd.
Received September 1994
Revised October 1995

Newtonian fluid by miniature pulsatile pumps. An increase in flow rate of non-Newtonian materials of the same pressure gradient is possible with pulsating flow as compared with steady flow. El Masry and El Shobaskys[13] reported that the energy saving can be as high 30% if an optimum frequency of pulsatile velocity is used. An experimental study of pulsatile flow in pipes within the transition range was made by Einav and Sokolov.[14] In the study of intracardiac blood flow and large vascular stenosis, pressure loss, maximum flow velocity and shear stress are parameters of interest because of their relation with the atheroma caused by a large pressure drop across the constriction, the corpuscle damage due to a large shear stress and the thrombus phenomena resulting from the recirculation region.[15–17]

The present investigation focused on the study of the development of the flow structure in pulsatile turbulent flow, the pressure losses in pulsating flow through constrictions, the characteristics of the maximum pulsatile flow velocity, the maximum values of vorticity and shear stress and the pulsatile velocity profiles. Empirical expressions were then formulated to better describe the relationships between the instantaneous flow rate (Q), the pressure loss (ΔP), the maximum velocity ($V_{\max}$), the maximum vorticity ($\zeta_{\max}$) and the maximum shear stress ($\tau_{\max}$) for turbulent pulsatile flow in the vicinity of constrictions in the pipe.

2. GOVERNING EQUATIONS AND NUMERICAL PROCEDURES

Incompressible turbulent flow in vascular pipes near a constriction is governed by the Reynolds-averaged Navier–Stokes equations. By using the eddy viscosity concept and the k–ε turbulence model closure, the dimensionless governing equations of two-dimensional flow can be expressed in axisymmetric co-ordinates as follows: continuity equation

$$\frac{\partial}{\partial z}(ru) + \frac{\partial}{\partial r}(rv) = 0, \tag{1}$$

z-momentum equation

$$St\frac{\partial u}{\partial t} + \frac{1}{r}\frac{\partial}{\partial z}(ru^2) + \frac{1}{r}\frac{\partial}{\partial z}(ruv) = -\frac{\partial p}{\partial z} + \frac{1}{r\partial z}\left(2r\nu_e\frac{\partial u}{\partial z}\right) + \frac{1}{r}\frac{\partial}{\partial r}\left[r\nu_e\left(\frac{\partial u}{\partial r} + \frac{\partial v}{\partial z}\right)\right], \tag{2}$$

r-momentum equation

$$St\frac{\partial v}{\partial t} + \frac{1}{r}\frac{\partial}{\partial z}(ruv) + \frac{1}{r}\frac{\partial}{\partial r}(rv^2) = -\frac{\partial p}{\partial r} + \frac{1}{r}\frac{\partial}{\partial z}\left[r\nu_e\left(\frac{\partial v}{\partial z} + \frac{\partial u}{\partial r}\right)\right] + \frac{1}{r}\frac{\partial}{\partial r}\left(2r\nu_e\frac{\partial u}{\partial r}\right) - \nu_e\frac{2v}{r^2}, \tag{3}$$

turbulent kinetic energy equation

$$St\frac{\partial k}{\partial t} + \frac{1}{r}\frac{\partial}{\partial z}(ruk) + \frac{1}{r}\frac{\partial}{\partial r}(rvk) = \frac{1}{r}\frac{\partial}{\partial z}\left(r\frac{\nu_t}{\sigma_k}\frac{\partial k}{\partial z}\right) + \frac{1}{r}\frac{\partial}{\partial r}\left(r\frac{\nu_t}{\sigma_k}\frac{\partial k}{\partial r}\right) + \nu_t G - \varepsilon, \tag{4}$$

turbulent dissipation rate equation

$$St\frac{\partial \varepsilon}{\partial t} + \frac{1}{r}\frac{\partial}{\partial z}(ru\varepsilon) + \frac{1}{r}\frac{\partial}{\partial r}(rv\varepsilon) + \frac{1}{r}\frac{\partial}{\partial z}\left(r\frac{\nu_t}{\sigma_\varepsilon}\frac{\partial \varepsilon}{\partial z}\right) + \frac{1}{r}\frac{\partial}{\partial r}\left(r\frac{\nu_t}{\sigma_\varepsilon}\frac{\partial \varepsilon}{\partial r}\right) + \nu_t C_1\frac{\varepsilon}{k}G - C_2 f_c\frac{\varepsilon^2}{k}. \tag{5}$$

The effective viscosity ν_e is defined as

$$\nu_e = \nu_t + 1/Re, \tag{6}$$

where $1/Re$ represents the contribution of the fluid molecular viscosity and ν_t is the dimensionless turbulent eddy viscosity defined by

$$\nu_t = C_\mu k^2/\varepsilon. \tag{7}$$

The variable G in the source terms of the k–ε equations is given as

$$G = 2\left[\left(\frac{\partial u}{\partial z}\right)^2 + \left(\frac{\partial v}{\partial r}\right)^2 + \frac{v^2}{r^2}\right] + \left(\frac{\partial u}{\partial r} + \frac{\partial v}{\partial z}\right)^2. \tag{8}$$

The values of the five empirical constants in the k–ε equations are[17,18]

$$C_\mu = 0{\cdot}09, \qquad C_1 = 1{\cdot}44, \qquad C_2 = 1{\cdot}92, \qquad \sigma_k = 1{\cdot}0, \qquad \sigma_\varepsilon = 1{\cdot}3.$$

The parameter f_c in the ε-equation represents the streamline curvature correction for the standard k–ε model and is defined as[19,20]

$$f_c = 1{\cdot}0 - C_c Ri_t, \qquad C_c = 0{\cdot}2, \qquad Ri_t = \frac{k^2}{\varepsilon^2}\frac{u^2 + v^2}{R_c^2}, \tag{9}$$

where Ri_t is the turbulent Richardson number and R_c is the local radius of streamline curvature given by

$$R_c = \left[uv\left(\frac{\partial v}{\partial r} - \frac{\partial u}{\partial z}\right) + u^2\frac{\partial v}{\partial z} - v^2\frac{\partial u}{\partial r}\right] \Big/ \left(u^2 + v^2\right)^{15}. \tag{10}$$

In the numerical process these equations are reformulated in a curvulinear co-ordinate system with the axisymmetric physical components taken as the dependent variables. Using the co-ordinate transformation

$$r = r(\xi, \eta), \qquad z = z(\xi, \eta), \tag{11}$$

the expressions for the Jacobian and contravariant metric tensor components are then given by

$$J = \xi_z\eta_r - \xi_r\eta_z, \qquad g^{11} = \xi_z^2 - \xi_r^2, \qquad g^{12} = \xi_z\eta_z - \xi_r\eta_r, \qquad g^{21} = g^{12}, \qquad g^{22} = \eta_z^2 - \eta_r^2. \tag{12}$$

The curvilinear velocity components (U, V) have a relation with the axisymmetric velocity (u, v) as

$$U = u\xi_z + v\xi_r, \qquad V = u\eta_z + v\eta_r. \tag{13}$$

Hence the transformed equations can be expressed in the general semi-strong conservation form[16,21]

$$\frac{\partial G}{\partial t} + \frac{\partial}{\partial \xi}(E - M) + \frac{\partial}{\partial \eta}(F - N) - S = 0, \tag{14}$$

where

$$G = St \cdot Jr(0, u, v, k, \varepsilon)^{\mathrm{T}}, \qquad E = Jr(U, uU + P\xi_z, vU + P\xi_r, kU, \varepsilon U)^{\mathrm{T}},$$
$$F = Jr(V, uV + P\eta_z, vV + P\eta_r, kV, \varepsilon V)^{\mathrm{T}},$$
$$M = Jr(M_1, M_2, M_3, M_4, M_5)^{\mathrm{T}}, \qquad N = Jr(N_1, N_2, N_3, N_4, N_5)^{\mathrm{T}},$$
$$S = Jr(S_1, S_2, S_3, S_4, S_5)^{\mathrm{T}},$$

$$M_1 = 0, \qquad M_2 = \nu_e\left[(g^{11} + \xi_r^2)u_\xi + (g^{12} + \xi_z\eta_z)u_\eta + \xi_z\xi_r v_\xi + \xi_r\eta_z v_\eta\right],$$
$$M_3 = \nu_e\left[(g^{11} + \xi_r^2)v_\xi + (g^{12} + \xi_r\eta_r)u_\eta + \xi_z\xi_r u_\xi + \xi_z\eta_r v_\eta\right],$$
$$M_4 = \frac{\nu_t}{\sigma_k}(g^{11}k_\xi + g^{12}k_\eta), \qquad M_5 = \frac{\nu_t}{\sigma_k}(g^{11}\varepsilon_\xi + g^{12}\varepsilon_\eta),$$

$$N_1 = 0, \qquad N_2 = \nu_e\left[(g^{21} + \xi_\xi\eta_z)u_\xi + (g^{22} + \eta_z^2)u_\eta + \xi_z\eta_r v_\xi + \eta_r\eta_z v_\eta\right],$$
$$N_3 = \nu_e\left[(g^{21} + \xi_r\eta_r)v_\xi + (g^{22} + \eta_r^2)v_\eta + \xi_r\eta_z u_\xi + \eta_z\eta_r u_\eta\right],$$
$$N_4 = \frac{\nu_t}{\sigma_k}(g^{21}k_\xi + g^{22}k_\eta), \qquad N_5 = \frac{\nu_t}{\sigma_\varepsilon}(g^{21}\varepsilon_\xi + g^{22}\varepsilon_\eta),$$

$$S_1 = 0, \qquad S_2 = 0, \qquad S_3 = \frac{p}{r} - \nu_e\frac{2v}{r^2}, \qquad S_4 = \nu_t G^* - \varepsilon, \qquad S_5 = \nu_t C_1 f_c G^*\frac{\varepsilon}{k} - C_2\varepsilon\frac{\varepsilon}{k}.$$

The non-linear equations (14) are solved by an iterative process. All the physical variables (u, v, p, k, ε) are updated as

$$\phi^{n+1} = \phi^n + \delta\phi, \tag{15}$$

where n and $n+1$ are the previous and current iteration numbers respectively and ϕ represents each of the physical variables. Substituting equation (15) into equation (14), the governing equations are then expressed in incremental form. The resulting equations are solved by the SIMPLE algorithm of Patankar[18] on a collocated non-staggered grid for ease of imposing the pressure boundary conditions. All terms containing incremental variables are discretized by three-point difference schemes: a first-order hybrid upwind difference scheme for convective terms, a second-order central scheme for diffusive terms, a first-order forward scheme for pressure terms and a first-order backward scheme for continuity equations. The residuals (R) are calculated by second-order difference schemes: a second-order upwind scheme for convective terms, a central scheme for diffusive terms and a second-order forward or backward scheme for pressure terms and continuity equations. Owing to the variation in the main flow direction in pulsatile flows, the discretizations of pressure gradient terms and continuity equations are adjusted according to the instantaneous main flow direction. A modified Crank–Nicolson scheme with a weighting factor θ is used to discretize the time-dependent terms in the governing equations. In the present work, $\theta = 0{\cdot}6$ was adopted after a series of numerical tests. The values of time step increment Δt chosen follow closely the general CFL criteria. At convergence the residual vector R approaches zero and the convergent results approach second-order accuracy.

3. GEOMETRICAL CONFIGURATION AND BOUNDARY CONDITIONS

The geometrical parameters are defined in Figure 1(a). The constriction has an opening ratio of 0·5 and a thickness ratio of 0·1. The grid points in the r-direction are equally distributed. A stretching function is used for the grid point distribution in the z-direction, as shown in Figure 1(b). Grid independence tests show that a grid size of 41 × 201 ($r \times z$) is sufficient for the present range of flow investigations.

In the solution domain shown in Figure 1(a) the velocity profile at the upstream inlet boundary is described by

$$u(r, t) = \frac{(n+1)(2n+1)}{2n^2}\bar{u}(t)\left(1 - 2\frac{r}{D}\right)^{1/n}, \tag{16}$$

where n is given a value of 6·0 in the present study. This power law rather than a parabolic profile is used at every time step, because the velocity profiles of pulsatile flow are generally not parabolic. The average inlet velocity $\bar{u}(t)$ is specified according to the type of pulsatile flow as shown in Figure 2: type I—pure sinusoidal flow, $\bar{u}_{\sin}(t) = \sin(2\pi t/T_{\sin})$; type II—physiological flow, $\bar{u}_{\text{phys}}(t)$;[3,22,23] type III—experimental pulsatile flow, $\bar{u}_{\text{exper}}(t)$, simulating the operation of a mechanical aortic valve.[1,24]

At each time step along the solid wall the no-slip velocity condition is used, i.e. $u = 0$ and $v = 0$. Along the centreline, axisymmetric conditions are applied for all variables, i.e. $\partial u/\partial r = 0$, $v = 0$, $\partial p/\partial r = 0$, $\partial k/\partial r = 0$ and $\partial \varepsilon/\partial r = 0$. At the downstream exit section the pressure is fixed at zero. The flow is considered to be fully developed, so the first-order differentials of all other variables along the z-direction are set to zero. The boundary conditions at the inlet section and the k and ε wall boundary conditions are described as follows.

The values of k and ε at the inlet section are given by[25]

$$k = C_\mu^{-1/2} l_m^2 \left(\frac{\partial u}{\partial r}\right)^2, \qquad \varepsilon = C_\mu^{1/2} k \frac{\partial u}{\partial r}, \tag{17}$$

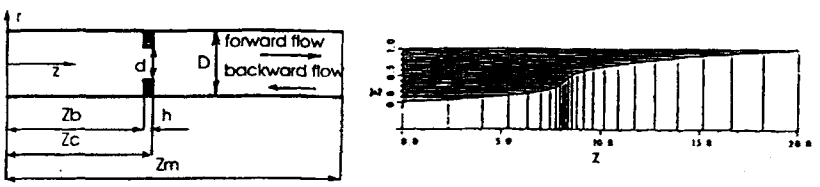

(a) geometrical parameters (b) grid distribution in z-direction

Figure 1. Configuration of pipe with ring-type constriction

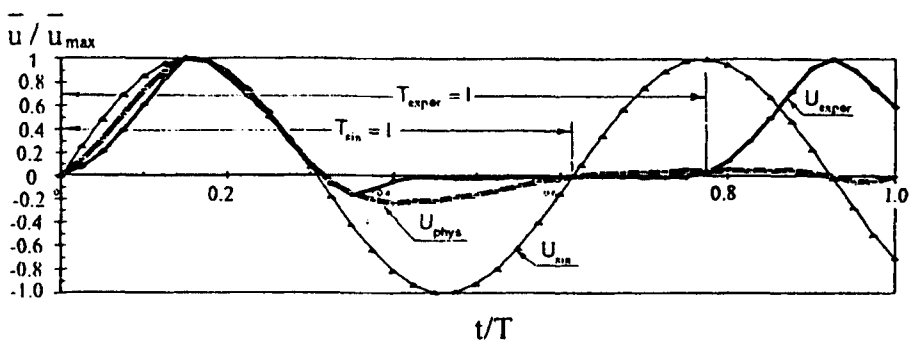

Figure 2. Three types of pulsatile flow

where the mixing length l_m is the smaller value either determined by the Nikuradse formula

$$\frac{l_m}{D} = 0{\cdot}07 - 0{\cdot}04\left(1 - \frac{2y}{D}\right)^2 - 0{\cdot}03\left(1 - \frac{2y}{D}\right)^4 \tag{18a}$$

or computed from the wall region formula

$$l_m = 0{\cdot}41y, \tag{18b}$$

where y is the normal distance from the wall. These formulations give zero values for k and ε at the centre of the vascular pipe, which is not realistic. To compensate for the possibility of unrealistic centreline values, a minimum value of the turbulent intensity of $0{\cdot}003\bar{u}(t)$ was determined.[25] A long computational vascular pipe region upstream of the constriction is also used in the present calculation to minimize this effect.

Along the solid wall a wall function is used to obtain the values of k and ε at those grid points adjacent to the solid wall. Dou[26] proposed an analytical function to connect u^*, u_p and y^+ for the whole flow region as follows (and as shown in Figure 3):

$$\frac{u_p}{u^*} = 2{\cdot}5\ln\left(1 + \frac{y^+}{5}\right) + 7{\cdot}05\left(\frac{y^+/5}{1 + y^+/5}\right)^2 + 2{\cdot}5\left(\frac{y^+/5}{1 + y^+/5}\right) - B^*, \tag{19}$$

where B^* represents the effect of wall roughness and is equal to zero in the present study and u_p is the velocity component parallel to the solid wall. The values of k and ε at the corresponding grid points are then calculated as

$$k = u^* 2/\sqrt{C_\mu}, \qquad \varepsilon = \lambda u^* 3/0{\cdot}41y, \qquad \nu_t = C_\mu k^2/\varepsilon, \tag{20}$$

where

$$\lambda = \frac{2}{1 + 5/y^+} + 0{\cdot}008(23{\cdot}2 - y^+)y^+ \Big/ \left(1 + \frac{y^+}{5}\right)^3.$$

4. RESULTS AND DISCUSSIONS

The results presented here are focused on cases corresponding to intracardiac flow and valvular regurgitation. The blood can be considered as a Newtonian fluid in the larger artery, where the shear rate is larger.[15,17,27] At 36–37 °C the blood density ρ is $1{\cdot}055 \times 10^3$ kg m^{-3} and the kinematic viscosity ν is 0·04 P or $3{\cdot}79 \times 10^{-6}$ m^2 s^{-1}. The peak velocity at the mitral valve opening section is about 3·0–6·0 m s^{-1}. The artery diameter is about $(2{\cdot}0–3{\cdot}0) \times 10^{-2}$ m and the corresponding peak Reynolds number Re is of the order of 10^4. The normal physiological frequency is about 72 beats per minute or 1·2 Hz, which gives a corresponding Womersley number $Nw = D\sqrt{(\omega/\nu)}$ of the order of 50·0. The above range of parameters was considered in the present study. Only the general trends of the results are presented in this paper.

4.1. *Turbulent pulsatile flow in tube with ring-type constriction*

Flow development. The general flow development of pulsatile flow is illustrated here for the case of $Re = 10^4$, $Nw = 50$ and $St = 0{\cdot}0398$. The sinusoidal, physiological and experimental pulsatile flow developments are presented in Figures 3–5 respectively. For each pulsatile flow the calculation was carried out for more than one complete periodic cycle. Within the interval $0{\cdot}0 < t/T \leqslant 20/65$, when the mean flow decreases to zero, the recirculation region on the downstream side of the constriction usually grows larger. This is shown through the development of the streamlines of the flow. In the flow

field, observations show that when the turbulent energy increases, the laminar cores of the flow field become smaller. This can also be observed from the shear stress contours presented in Figures 3(b)–5(b). For $20/65 < t/D \leqslant 30/65$ the flow generally reverses towards the negative z-direction. The differences in the pulsatile flow characteristics of the three types of pulsatile flow simulation appear to be mainly due to the differences in their original mean velocity fields given in Figure 2. At the beginning of the reverse flow the region of larger turbulent shear stress is generally located at the right side of the constriction at $t/T = 22/65$, $26/65$ and $26/65$ for the sinusoidal (Figure 3), physiological (Figure 4) and experimental (Figure 5) pulsatile flows respectively. The region with large turbulent shear stress moves gradually to the left side of the constriction for both the sinusoidal and physiological flows, but it is generally located on the right side of the constriction for the experimental pulsatile flow. For $20/65 < t/D \leqslant 30/65$ the recirculation region of the pulsatile flow field generally developed towards the left side for all pulsatile flows. In the subsequent time steps the left side of the recirculation region grew larger for the sinusoidal and physiological flows than for the experimental pulsatile flow field.

Centreline velocity (V_c) and turbulent kinetic energy (k_c). The centreline velocity is an important parameter in the study of pulsatile flow fields. For every two time steps the centreline velocity and centreline turbulent kinetic energy distributions along the z-direction are presented in Figures 6–8 for the case of $Re = 10^4$, $Nw = 50$ and $St = 0{\cdot}0398$ for each of the pulsatile flows.

The characteristics of the V_{max} and k_c distributions along the axial direction are similar between the physiological and experimental pulsatile flows, as shown in Figures 7 and 8 for the case of $Nw = 50$ and $St = 0{\cdot}0398$. The maximum foward V_c-value is equal to 5·1 for both types of pulsatile flow. The maximum k_c-value is about 0·9. During the small time intervals $42/65 < t/T \leqslant 1{\cdot}0$ and $42/65 < t/T \leqslant 52/65$ the fluid is nearly stationary and the turbulent kinetic energy diminishes completely to zero. Hence for these two pulsatile flow fields there exist both laminar and turbulent flow characteristics over a complete cyclic period.

4.2. Parametric relations of turbulent pulsatile flows in pipe with ring-type constriction

Relation between flow rate (Q) and instantaneous maximum values of velocity (V_{max}), turbulent kinetic energy (k_{max}) and turbulent viscosity ($\nu_{t,max}$). A linear relationship between the flow rate Q and the maximum flow velocity V_{max} exists. This is shown in Figure 9 for the case of $Nw = 50$ and $St = 0{\cdot}0398$. All three types of pulsatile flow exhibit a similar linear relation of the form

$$V_{max} = C_{vm} Q, \tag{21}$$

where $C_{vm} = 6{\cdot}80$ in the present study. The instantaneous maximum velocity reaches its peak value at the same time as the instantaneous flow rate. The phase angle between these two parameters is equal to zero.

The relation between the flow rate Q and the maximum turbulent kinetic k_{max} is not linear (Figure 10). At the same flow rate, during the acceleration period the instantaneous k has a smaller value of k_{max} for all three pulsatile flows. This implies that the acceleration tends to suppress the development of fluid disturbances. For the sinusoidal flow the effect of the initial fluid stationary condition was not felt until after one-quarter of a cycle, as shown in Figure 10(b). Symmetrical flow phenomena exist between the forward and backward parts of the pulsatile flow characteristics shown in Figure 10(b). At $Q = 0{\cdot}0$, k_{max} is not equal to zero but has a value of 0·015. This property of the sinusoidal flow is different from the other two pulsatile flows, where $k_{max} = 0$ at $Q = 0$.

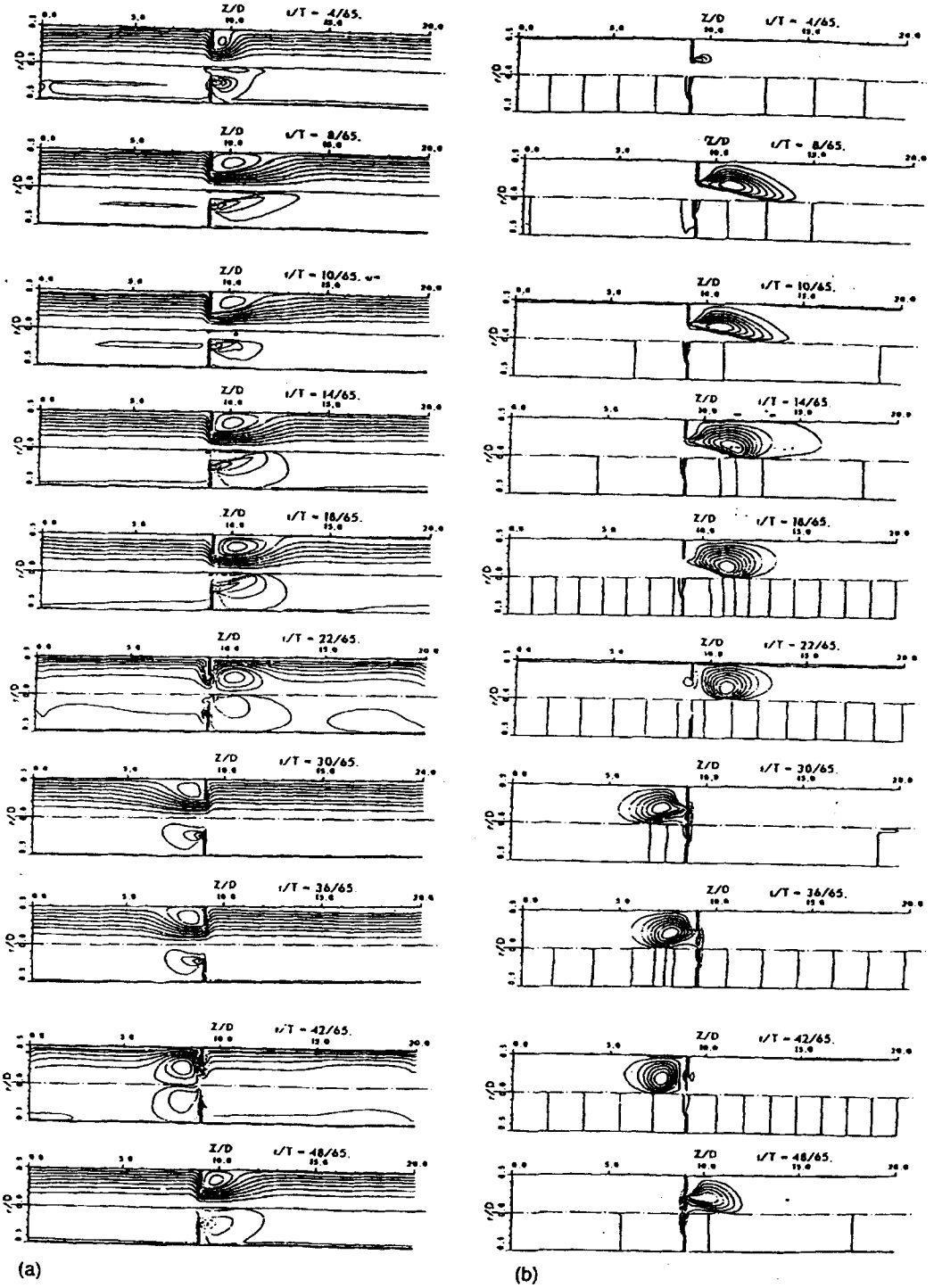

Figure 3. Sinusoidal turbulent flow field development in pipe with ring-type constriction for $Re = 10^4$, $Nw = 50$, $St = 0{\cdot}0398$ and $d/D = 0{\cdot}5$, $h/D = 0{\cdot}1$. (a) Streamlines (upper half) and vorticity contours (lower half). (b) Shear stress (upper half) and isobar (lower half)

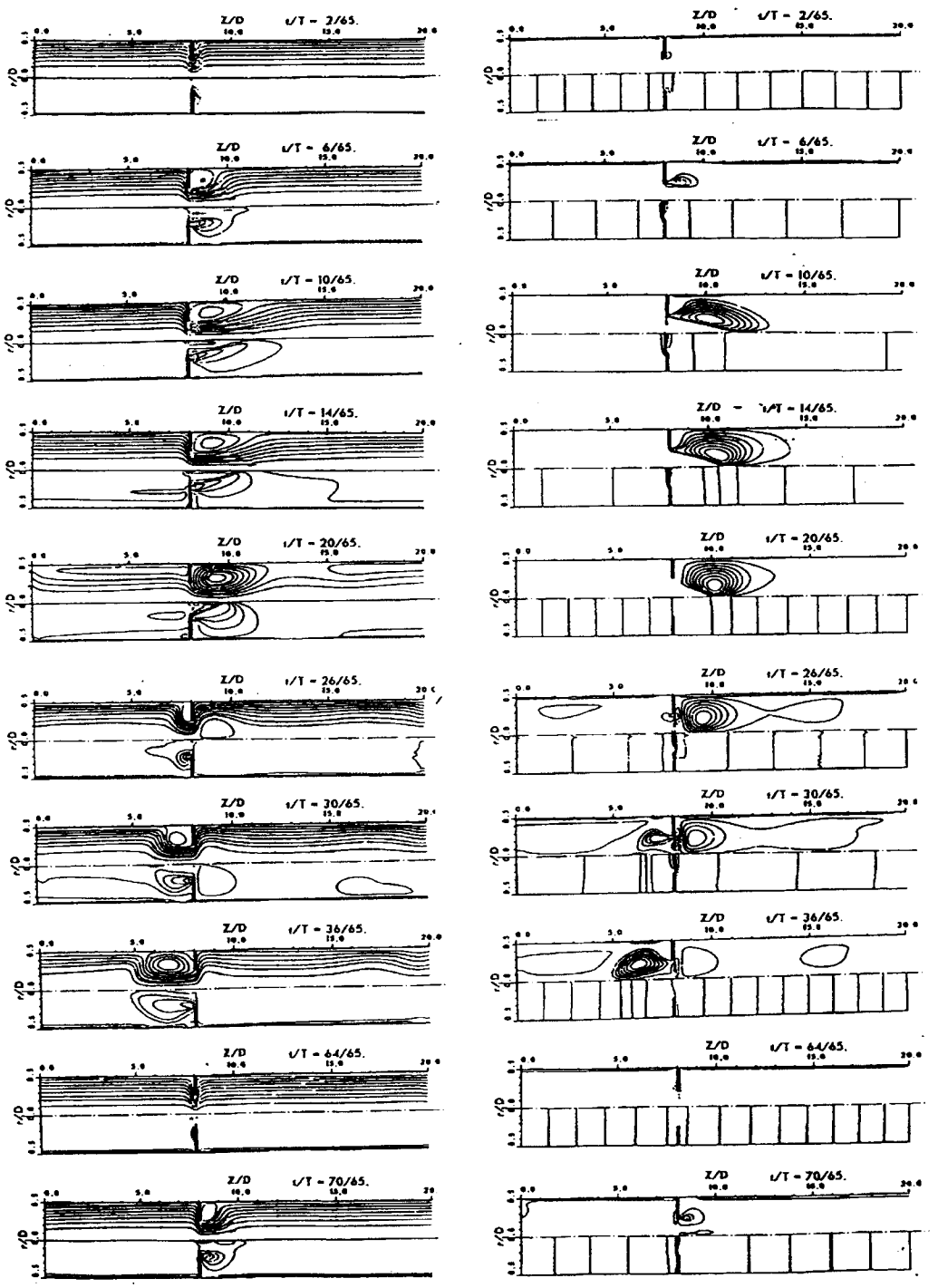

Figure 4. Physiological turbulent flow field development in pipe with ring-type constriction for $Re = 10^4$, $Nw = 50$, $St = 0{\cdot}0398$ and $d/D = 0{\cdot}5$, $h/D = 0{\cdot}1$. (a) Streamlines (upper half) and vorticity contours (lower half). (b) Shear stress (upper half) and isobar (lower half)

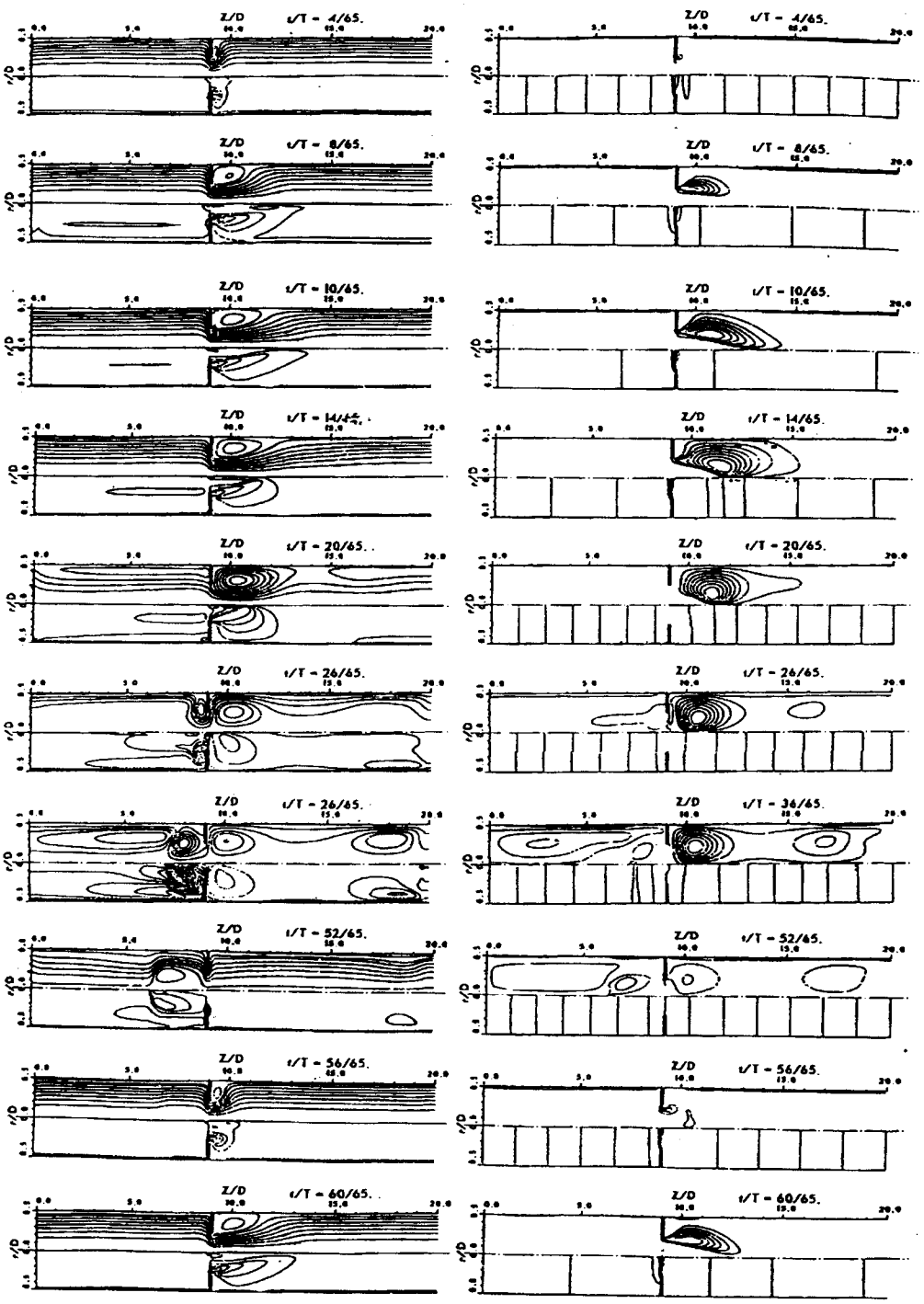

Figure 5. Experimental pulsatile turbulent flow in pipe with ring-type constriction for $Re = 10^4$, $Nw = 50$, $St = 0{\cdot}0398$ and $d/D = 0{\cdot}5$, $h/D = 0{\cdot}1$. (a) Streamlines (upper half) and vorticity contours (lower half). (b) Shear stress (upper half) and isobar (lower half)

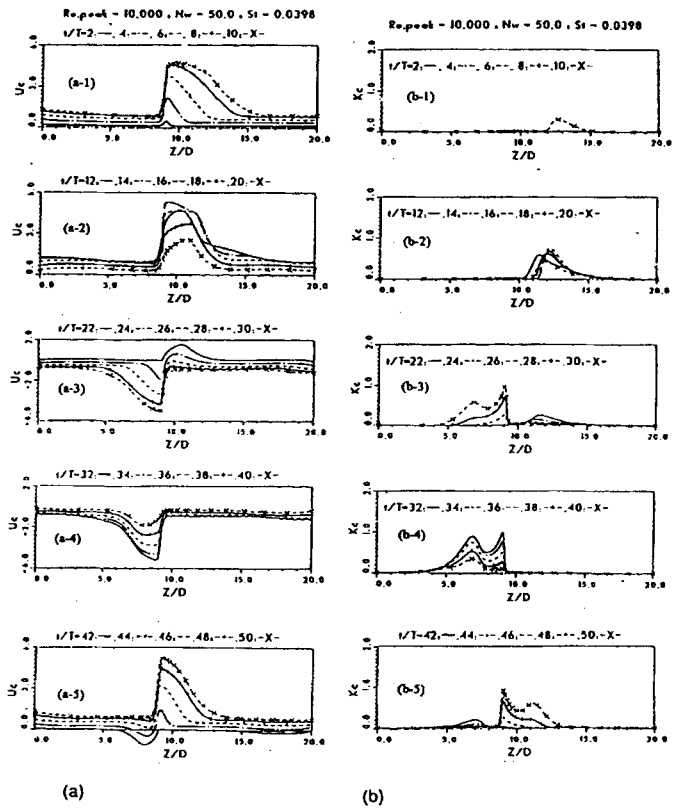

Figure 6. Sinusoidal turbulent flow in pipe with constriction of $d/D = 0{\cdot}5$, $h/D = 0{\cdot}1$ and $Re = 10^4$, $Nw = 50$, $St = 0{\cdot}0398$. (a) Centreline velocity. (b) Centreline turbulent kinetic energy

The development of the characteristics of turbulence in the pulsatile flow field with time can be deduced from the relationship between the flow rate Q and the maximum turbulent viscosity $\nu_{t,max}$ as shown in Figure 11. For the sinusoidal flow, $\nu_{t,max}$ is consistently larger than zero, except during the starting phase of the pulsatile flow period. The flow in general has a smaller $\nu_{t,max}$ during the acceleration period than during the deceleration period. The flow is in general turbulent for the sinusoidal flow, with a minimum instantaneous $\nu_{t,max}$ of the order of 0·016. For the physiological and experimental pulsatile flows, $\nu_{t,max} = 0{\cdot}0$ for $0 < Q < 0{\cdot}3$ within a small time interval at each of the periodic cycles. Hence these flows show transitional characteristics of laminar-to- turbulent and turbulent-to-laminar flow developments in every pulsating cycle.

Relation between flow rate (Q) and pressure loss (P_{loss}). The relation between the flow rate Q and the pressure loss P_{loss} is quadratic in nature, as shown in Figure 12. The peak non-dimensional P_{loss} is about 10·5 at the maximum instantaneous flow rate. The phase angle between the two parameters is equal to zero. Curve fitting for the three pulsatile flows gives a relationship of the form

$$P_{loss} = C_{pl} Q|Q|, \tag{22}$$

where $C_{pl} = 17{\cdot}9$. Equation (22) is plotted in Figure 12 as the full curve.

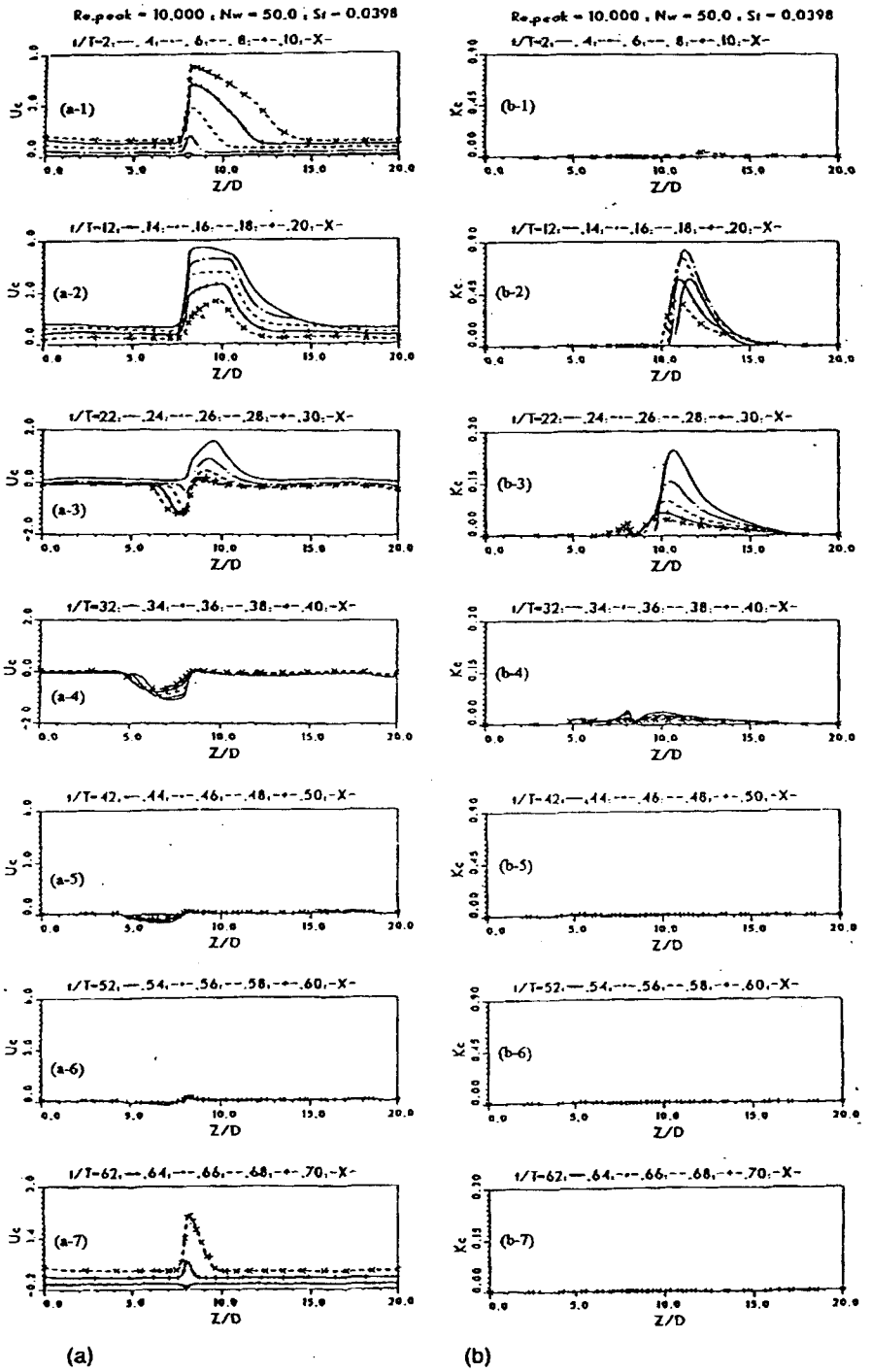

Figure 7. Physiological turbulent flow in pipe with constriction of $d/D=0{\cdot}5$, $h/D=0{\cdot}1$ and $Re=10^4$, $Nw=50$, $St=0{\cdot}0398$. (a) The centreline velocity. (b) The centreline turbulent kinetic energy

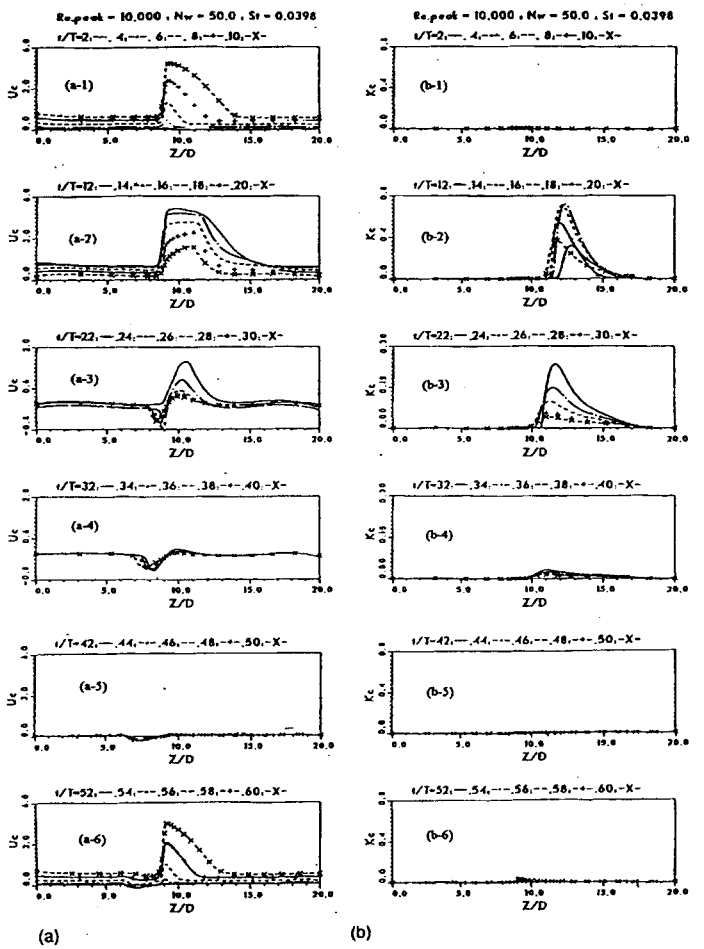

Figure 8. Experimental pulsatile turbulent flow in pipe with constriction of $d/D=0{\cdot}5$, $h/D=0{\cdot}1$ and $Re=10^4$, $Nw=50$, $St=0{\cdot}0398$. (a) The centreline velocity. (b) The centreline turbulent kinetic energy

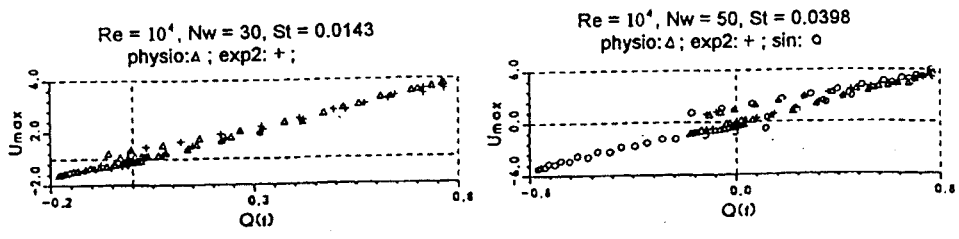

(a) At Nw = 30, St = 0.0143 (b) At Nw = 50, St = 0.0398

Figure 9. Relation between flow rate and maximum flow velocity of flow in pipe with constriction of $d/D=0{\cdot}5$, $h/D=0{\cdot}1$ and $Re=10^4$

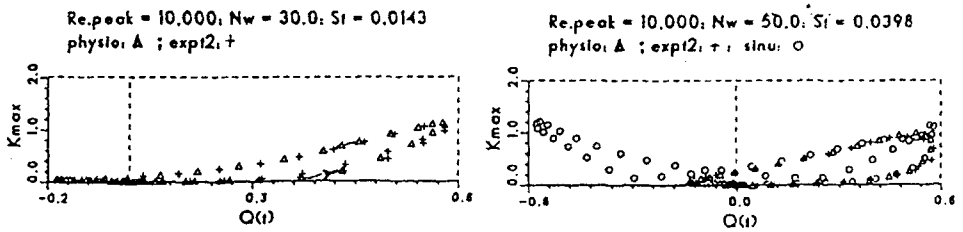

(a) At Nw = 30, St = 0.0143 (b) At Nw = 50, St = 0.0398

Figure 10. Relation between flow rate and maximum turbulent kinetic energy of flow in pipe with constriction of $d/D=0{\cdot}5$, $h/D=0{\cdot}1$ and $Re=10^4$

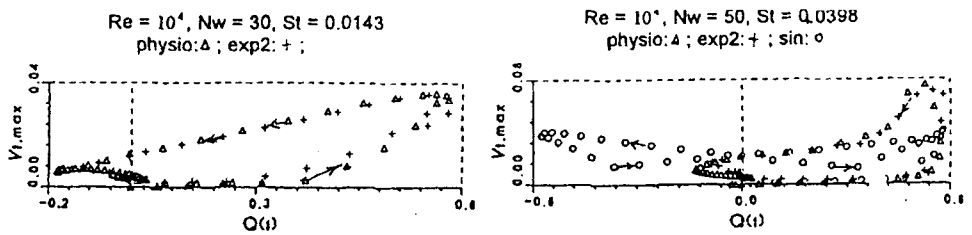

(a) At Nw = 30, St = 0.0143 (b) At Nw = 50, St = 0.0398

Figure 11. Relation between flow rate and maximum turbulent viscosity of flow in pipe with constriction of $d/D=0{\cdot}5$, $h/D=0{\cdot}1$ and $Re=10^4$

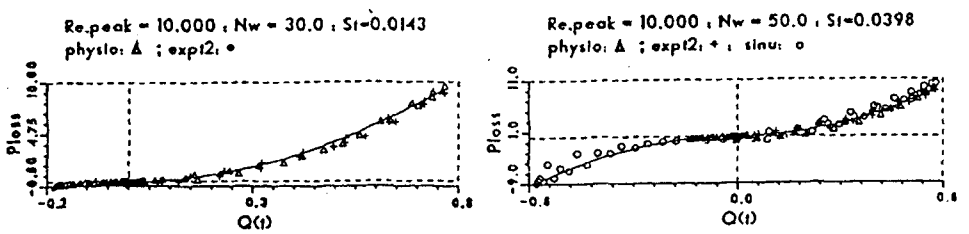

(a) At Nw = 30, St = 0.0143 (b) At Nw = 50, St = 0.0398

Figure 12. Relation between flow rate and pressure loss of flow in pipe with constriction $d/D=0{\cdot}5$, $h/D=0{\cdot}1$ and $Re=10^4$

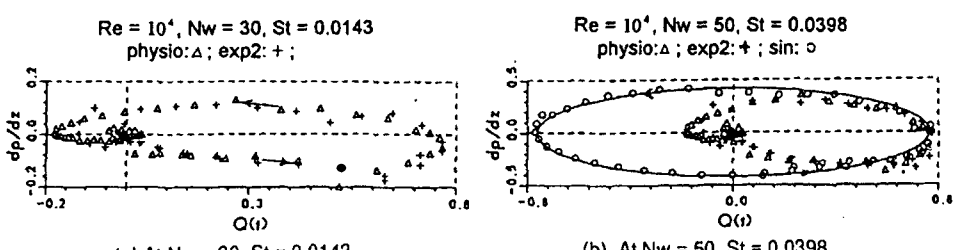

(a) At Nw = 30, St = 0.0143 (b) At Nw = 50, St = 0.0398

Figure 13. Relation between flow rate and pressure gradient of flow in pipe with constriction of $d/D=0{\cdot}5$, $h/D=0{\cdot}1$ and $Re=10^4$

Relation between flow rate (Q) and pressure gradient (dp/dz). The relation between the flow rate Q and the pressure gradient dp/dz along the axial direction in the fully developed region is presented in Figure 13. The phase angle between these two parameters is 90°. The peak dp/dz appears at the instant of zero flow rate ($Q=0$), when the flow has its maximum acceleration or deceleration. Conversely, $dp/dz=0$ occurs at the instant of maximum flow rate, when the flow acceleration is equal to zero. Hence the characteristics of dp/dz depend mainly on the flow acceleration or deceleration. The pressure gradient has the same absolute values for the same acceleration and deceleration. For the sinusoidal flow this relation can be expressed as

$$\left(\frac{dp/dz}{C_{pz1}}\right)^2+\left(\frac{Q}{C_{pz2}}\right)^2=1, \tag{23}$$

where $C_{pz1}=0{\cdot}4$ and $C_{pz2}=0{\cdot}785$ for the present study. Equation (23) is plotted in Figure 13(b) as the full curve.

Relation between flow rate (Q) and maximum values of vorticity (Ω_{max}) *and wall vorticity* ($\Omega_{w,max}$). As shown in Figure 14, the maximum vorticity Ω_{max} is linearly related to the flow rate Q. For both $St=0{\cdot}0398$ and $0{\cdot}0143$ the relationship can be generally expressed as

$$\Omega_{max}=C_{\Omega m}Q, \tag{24}$$

where $C_{\Omega m}=240{\cdot}5$ in the present study.

A similar relation between Q and the maximum wall vorticity $\Omega_{w,max}$ is shown in Figure 15. In a complete cycle the peak wall vorticity $\Omega_{w,max}$ is less than $1/6$ of the maximum vorticity Ω_{max} of the whole flow field. $\Omega_{w,max}$ also has its peak value at the instant of maximum flow rate.

Relation between flow rate (Q) and maximum values of shear stress (τ_{max}) *and wall shear stress* ($\tau_{w,max}$). In physiological flow, turbulent shear stress is directly related to the cause of blood cell damage. The numerical results for the instantaneous maximum values of the turbulent shear stress τ_{max} of the whole flow field and the wall shear stress $\tau_{w,max}$ are presented in Figures 16 and 17 respectively. The relation between Q and τ_{max} is complex. For the same Q-value the τ_{max}-value is smaller during acceleration than during deceleration. This is similar to the phenomenon discussed in the turbulent viscosity development. The peak non- dimensional τ_{max} is $0{\cdot}48$ at the instant of maximum flow rate. The wall shear stress $\tau_{w,max}$ has a simple quadratic relationship with the flow rate. The three pulsatile flows investigated here show a similar relation for both $St=0{\cdot}0143$. It can generally be represented by

$$\tau_{w,max}=-C_{\tau wm}AQ|Q|, \tag{25}$$

where $C_{\tau wm}=0{\cdot}032$ in the present study. Equation (25) is plotted in Figure 17 as the full curve. Similarly to the vorticity values, the peak $\tau_{w,max}$ is much smaller than the overall turbulent shear stress and only about $1/25$ of the peak value of the overall maximum instantaneous maximum turbulent shear stress τ_{max}.

4.3. Application of present results to intracardiac flow

Consider the two parameters of pressure loss and turbulent shear stress for the case of $Re=10^4$ and $D=2{\cdot}5\times10^{-2}$ m. The dimensional pressure is given by

$$P_{loss}=4{\cdot}340\times10^4Q|Q|. \tag{26}$$

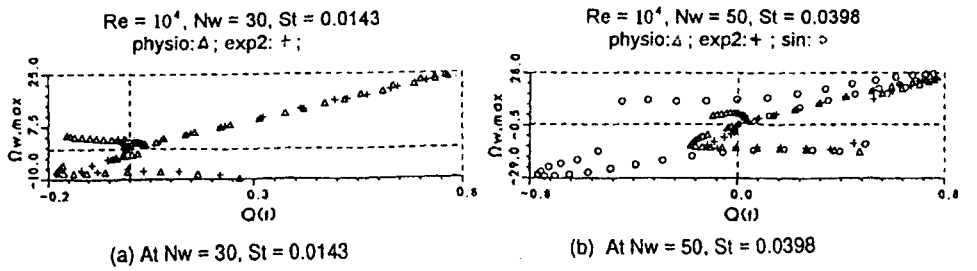

Figure 14. Relation between flow rate and maximum vorticity of flow in pipe with constriction of $d/D = 0{\cdot}5$, $h/D = 0{\cdot}1$ and $Re = 10^4$

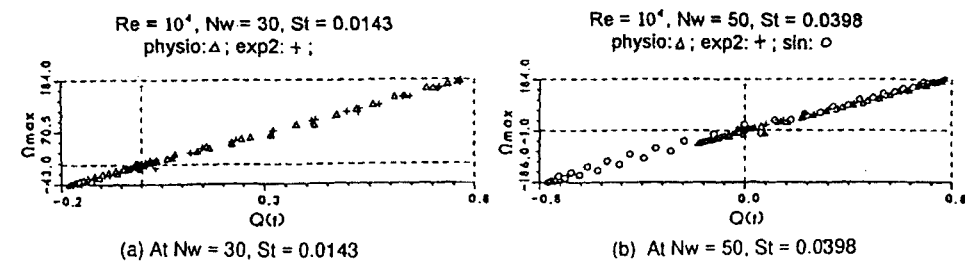

Figure 15. Relation between flow rate and maximum vorticity of flow in pipe with constriction of $d/D = 0{\cdot}5$, $h/D = 0{\cdot}1$ and $Re = 10^4$

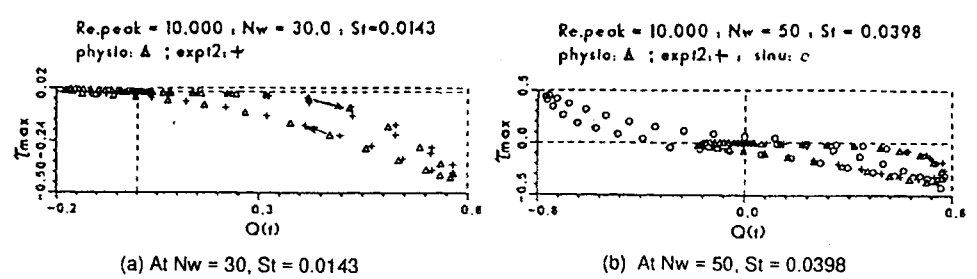

Figure 16. Relation between flow rate and maximum turbulent shear stress of flow in pipe with constriction of $d/D = 0{\cdot}5$, $h/D = 0{\cdot}1$ and $Re = 10^4$

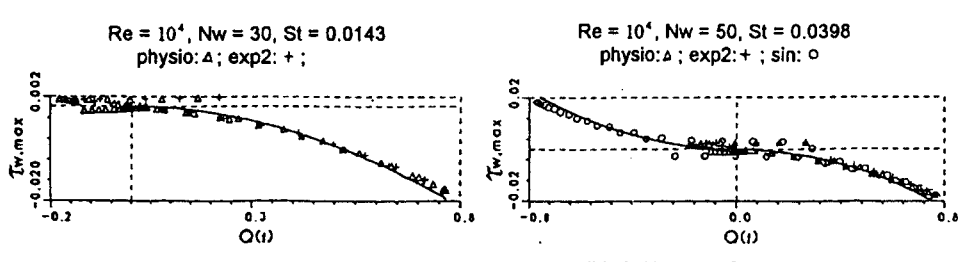

Figure 17. Relation between flow rate and maximum wall turbulent shear stress of flow in pipe with constriction of $d/D = 0{\cdot}5$, $h/D = 0{\cdot}1$ and $Re = 10^4$

The value of the peak pressure loss is $2{\cdot}674 \times 10^4$ N m^{-2} or 200·7 mmHg. This value is large enough to cause atheroma, which is developed at a pressure drop greater than 30 mmHg. At $Q = 0{\cdot}50_{max}$ the pressure drop is equal to 50·2 mmHg, which is also larger than the critical value.

The dimensional wall shear stress is given by

$$\tau_{w,max} = 77{\cdot}59Q|Q|. \tag{27}$$

The peak wall shear stress is equal to 47·81 N m^{-2}, which is close to the critical value of endothelium deterioration, 40 N m^{-2}. The peak dimensional turbulent shear stress is equal to $1{\cdot}115 \times 10^3$ N m^{-2}. This value is very much larger than the critical value of incipient haemolysis, 400 N m^{-2}. At $Q = 0{\cdot}50_{max}$ the turbulent shear stress is equal to 418·1 N m^{-2}, which is also greater than the critical value.

5. CONCLUSIONS

Three types of pulsatile turbulent flow in a vascular pipe with a ring-type constriction have been computed for a Reynolds number of the order of 10^4, Womersley numbers of 30 and 50 and corresponding Strouhal numbers of 0·0143 and 0·0398. The three pulsatile flows are a pure sinusoidal flow, a physiological flow and an experimental pulsatile flow profile for physiological flow simulations.

The sinusoidal pulsatile flow in the vicinity of a pipe with a ring-type constriction is observed to be always turbulent after the pulsatile flow is initiated. The flow disturbance is not diminished completely, because the time period with small velocity in each cycle is very short. The other two physiological-type non-symmetrical pulsatile flows investigated exhibit both laminar and turbulent flow characteristics in an alternating manner within the pulsatile flow fields. The length of the laminar core in the latter pulsatile flow, as shown through the turbulent shear stress contours, was observed to change in magnitude and domain with respect to time in a systematic manner.

Various parametric flow relationships are obtained to describe the pulsatile flow characteristics. Numerical linear relationships are found between the flow rate and the maximum values of velocity and vorticity. Quadratic relationships are obtained between the flow rate and the pressure loss across the constriction and between the flow rate the maximum wall shear stress. An elliptic relationship is observed between the flow rate and the pressure gradient. From the flow characteristics obtained, flow acceleration was observed to suppress the development of flow disturbance in the pulsatile flows studied here. All the instantaneous maximum values of turbulent kinetic energy, turbulent viscosity and turbulent shear stress are smaller during the acceleration phase than during the deceleration period.

APPENDIX: NOMENCLATURE

C_c, C_μ, C_1, C_2	coefficients of turbulence model
d	orifice diameter
D	vascular pipe diameter, used as characteristic length L
f_c	coefficient of turbulence model
h	obstacle height, $(D - d)/2$
k	dimensionless turbulent kinetic energy
Nw	Womersley number, $D\sqrt{(\omega/\nu)}$
p	dimensionless pressure
P_{loss}	dimensionless pressure loss
Q	flow rate, $\pi D^{2-}u(t)/4$
Q_{max}	maximum flow rate, $\pi/4$
r	radial co-ordinate, radial distance

Re	Reynolds number, $\bar{u}_{\text{peak}}D/\nu$
Ri_t	Richardson number of streamline curvature
St	Strouhal number, $D/\bar{u}_{\text{peak}}T=(1/2\pi)Nw^2/Re$
t	time co-ordinate
T	time period of physiological flow cycle
$T_{\sin}$	time period of sinusoidal flow cycle
u	dimensionless axial velocity component
$\bar{u}(t)$	instant average velocity in vascular pipe
$\bar{u}_{\text{peak}}$	peak $\bar{u}(t)$-value, characteristic velocity
v	dimensionless radial velocity component
z	axial co-ordinate, axial distance
z_r	recirculation length

Greek letters

ε	dimensionless dissipation rate of turbulent energy
ν_e	effective viscosity, $1/Re+\nu_t$
ν_t	turbulent eddy viscosity
ξ, η	co-ordinate variables in general curvature co-ordinate system
ρ	fluid density
τ	dimensionless shear stress, $\nu_e(\partial u/\partial r+\partial v/\partial z)$
ϕ_{p-Q}	phase angle between flow rate and pressure gradient variation in pulsatile flow
Ω	dimensionless vorticity, $\partial u/\partial r-\partial v/\partial z$

REFERENCES

1. L. H. Back, J. R. Radbill and Y. I. Cho, 'Measurement and prediction of flow through a replica segment of a mildly atherosclerotic coronary artery of man', *J. Biomech.*, **19**, 1–17 (1986).
2. J. S. Lee and Y. F. Fung, 'Flow in locally constricted tubes at low Reynolds numbers', *ASME J. Appl. Mech.*, **37**, 9–16 (1970).
3. J. S. Lee and Y. F. Fung, 'Flow in non-uniform small blood vessels', *J. Microvasc. Res.*, **3**, 272–287 (1971).
4. W. L. Oberkampf and S. C. Goh, 'Numerical solution of incompressible viscous flow in irregular tubes', *Proc. Int. Conf. on Computational Methods for Non-linear Mechanics*, 1974, pp. 569–579.
5. J. C. Bentz and N. A. Evans, 'Haemodynamic flow in the region of a simulated stenosis', *ASME Paper 75-WA/BA10-10*, 1975.
6. M. D. Deshpande, D. P. Giddens and R. F. Mabon, 'Steady laminar flow through modelled vascular stenoses', *J. Biomech.*, **9**, 165–174 (1976).
7. S. O. Wille, 'Pressure and flow in arterial stenoses simulated in mathematical models', *Appl. Math. Model.*, **4**, 483–488 (1980).
8. V. O'Brien and L. W. Erhlich, 'Simple pulsatile flow in an artery with a constriction', *J. Biomech.*, **18**, 117–127 (1985).
9. S. C. Dreumel and G. D. C. Kuiken, 'Steady flow through a double converging–diverging tube model for mild coronary stenoses', *J. Biomech. Eng.*, **111**, 212–221 (1989).
10. T. S. Lee, 'Numerical studies of fluid flow through tubes with double constrictions', *Int. j. numer. methods fluids*, **11**, 1113–1126 (1990).
11. T. S. Lee, 'Steady laminar fluid flow through variable constrictions in vascular tubes', *J. Fluids Eng.*, **116**, 66–71 (1994).
12. E. H. Jones Jr. and R. A. Bajura, 'A numerical analysis of pulsating laminar flow through a pipe orifice', *J. Fluids Eng.*, **113**, 199–205 (1991).
13. O. A. El Masry and K. El Shobakys, 'Pulsating slurry flow in pipelines', *Exp. Fluids*, **7**, 481–486 (1989).
14. S. Einav and M. Sokolov, 'An experimental study of pulsatile pipe flow in the transition range', *ASME J. Biomech. Eng.*, **115**, 404–411 (1993).
15. H. Huang, V. J. Modi, B. R. Seymour and R. Raliga, 'Fluid dynamics of stenosed arteries: a numerical study', *Proc. 6th Int. Conf. on Biomedical Engineering*, 1990, pp. 5352–540.
16. Z. Lou and W.-J. Yang, 'A computer simulation of the non-Newtonian blood flow at the aortic bifurcation', *J. Biomech.*, **26**, 37–49 (1993).
17. D. M. Stevenson, A. P. Yoganathan and F. P. Williams, 'Numerical simulation of steady turbulent flow through trifleat aortic heart valves—II. Results on five models', *J. Biomech.*, **18**, 909–926 (1985).
18. S. V. Patankar, *Numerical Heat Transfer and Fluid Flow*, Hemisphere, Washington, DC, 1980.

19. T. Tangsanchali and S. Maheswaran, '2-D depth-averaged flow computation near groyne', *J. Hydraul. Eng.*, **116**, 71–81 (1990).
20. S. K. Dong and M. K. Chung, 'Curvature corrections to Reynolds stress model for computation of turbulent recirculation flows', *AIAA J.*, **30**, 2968–2969 (1992).
21. M. Reggio, M. Agouzoul and R. Camarero, 'Computation of incompressible turbulent flows by an opposed-differencing scheme', *Numer. Heat Transfer*, **12**, 307–320 (1987).
22. D. A. McDonald, 'The relation of pulsatile pressure to flow in arteries', *J. Physiol.*, **127**, 533–552 (1955).
23. L. H. Back, J. R. Radbill and D. W. Crawford, 'Analysis of pulsatile, viscous blood flow through diseased coronary arteries of man', *J. Biomech.*, **10**, 339–353 (1977).
24. H. W. Sung and A. P. Yoganathan, 'Secondary flow velocity patterns in a pulmonary artery model with varying degrees of valvular pulmonic stenosis: pulsatile in-vitro studies', *ASME J. Biomech. Eng.*, **112**, 88– 92 (1990).
25. R. S. Amano and H. Brandt, 'Numerical study of turbulent axisymmetric jets impinging on a flat plate and flowing into an axisymmetric cavity', *ASME J. Fluids Eng.*, **106**, 410–417 (1984).
26. G. R. Dou, 'The turbulence structure of opening channel and pipe flows', *Sci. China*, **11**, 1115–1124 (1980) (in Chinese).
27. B. Diebold, A. Delouche, P. H. Dumee, J. P. Guglielmi, P. H. Delouche and P. Peronneau, 'In-vitro analysis of a model of intracardiac jet: analysis of the central core of axisymmetric jets', *J. Biomech.*, **23**, 35–44 (1990).